J Solid State Electrochem (2007) 11:1689–1695
DOI 10.1007/s10008-007-0330-4

ORIGINAL PAPER

Sensitively probing the cofactor redox species and photo-induced electron transfer of wild-type and pheophytin-replaced photosynthetic proteins reconstituted in self-assembled monolayers

Jingjing Xu · Yidong Lu · Baohong Liu · Chunhe Xu · Jilie Kong

Received: 22 January 2007 / Revised: 23 March 2007 / Accepted: 10 April 2007 / Published online: 23 May 2007

Abstract An ultrathin, ordered, and packed protein film, consisting of the 2-mercaptoacetic acid (MAA), polydimethyldiallylammonium chloride (PDDA), and wild-type (WT) photosynthetic reaction center (RC; termed as WT-RC) or its pheophytin (Phe)-replaced counterpart (termed as Phe-RC), was fabricated by self-assembling technique onto gold electrode for facilitating the electron transfer (ET) between RC and the electrode surface. Near-infrared (NIR)-visible (Vis) absorption and fluorescence (FL) emission spectra revealed the influence of pigment substitution on the cofactors arrangement and excitation relaxation of the proteins, respectively. Square wave voltammetry (SWV) and photoelectric tests were employed to systematically address the differences between the WT-RC films and mutant ones on the direct and photo-induced ET. The electrochemical results demonstrated that ET initiated by the oxidation of the primary donor (P) was obviously slowed down, and the formed P^+ had more population as well as more positive redox potential in the Phe-RC films compared with those in the WT ones. The photoelectrochemical results displayed the dramatically enhanced photoelectric performances of the mutant ones, further suggesting the slow-down formation of final charge-separated state in Phe-RC. The functionalized protein films introduced in this paper provided an efficient approach to sensitively probe the redox cofactors and ET differences resulting from only minor changes in pigment arrangement in the pigment–protein complex. The favored ET process observed for the membrane proteins RC was potentially valuable for a deep understanding of the multi-step biological ET process and development of versatile bioelectronic devices.

Keywords Photosynthetic reaction center · Self-assembled monolayers · Electron transfer · Square wave voltammetry · Photocurrent

J. Xu · Y. Lu · B. Liu · J. Kong
Chemistry Department and Institutes of Biomedical Sciences,
Fudan University,
Shanghai 200433, People's Republic of China

C. Xu
Shanghai Institute of Plant Physiology and Ecology,
Shanghai Institute for Biological Sciences,
Chinese Academy of Sciences,
Shanghai 200032, People's Republic of China

J. Kong (✉)
Department of Chemistry, Fudan University,
Shanghai 200433, People's Republic of China
e-mail: jlkong@fudan.edu.cn

Introduction

Bacteria photosynthetic reaction center (RC) from *Rhodobacter sphaeroides*, a simple but robust transmembrane pigment–protein complex primarily building up a light-driven electrical potential across the bacteria photosynthetic membrane, has been served typically as a valuable model system for probing the biological electron transfer (ET) process [1, 2]. Sparked by the nearly 100% quantum yield of the photo-induced charge separation of RC [3, 4], many efforts have been made to explore the long-range ET behavior both theoretically and experimentally [5–26]. The photo-induced ET process of RC is triggered upon photoexcitation of the primary electron donor (P) cofactor,

a bacteriochlorophyll (Bchl) dimer, and terminates in the ET between the primary quinone (Q_A) cofactor and the secondary quinone (Q_B). The accessory Bchl and bacteriopheophytin (Bphe) cofactors also participate in the initial ET steps as indispensable electron acceptors. Noticeably, despite that most of the cofactors noncovalently bound in the protein matrix are arranged twofold symmetrically, the ET only occurs unidirectionally along the L-branch [5, 6] (see Scheme 1a for details).

Electrochemical technique was addressed as an effective way to characterize electroactive species and probe ET processes in biological systems. The redox properties of the cofactors inside RC suggested the employment of such methods to reveal the energetics and pathways of the sequential ET behavior [11]. Agostiano et al. [12] reported previously the use of several electrochemical methods, including chronoamperometry, cyclic voltammetry (CV), and linear sweep voltammetry, to study the interactions between the different mediators and RC. Voltammetric peaks for RC in thin lipid films prepared on pyrolytic graphite (PG) electrodes were then investigated by Munge et al. [13]. In our previous work [15, 16], direct electrochemistry was realized for RC reconstituted in polycation sandwiched monolayer, permitting the determination of the redox cofactors midpoint potential (E_m), an important parameter relating to the driving force of the ET reactions, by CV and square wave voltammetry (SWV). Further study on SWV, bulk electrolysis, and photoelectric tests of the RC self-assembled monolayers (SAMs) demonstrated the dramatically different orientations of the proteins on Au electrodes linked by different bifunctional reagents [17].

Recently, site-directed mutagenesis and pigments replacement were widely adopted for a deep understanding of the complicated ET process in RC [19–26]. The specific treatments of RC brought about obvious alterations on E_m of the cofactors and thus influenced the ET significantly. A typical example was the incorporation of plant pheophytin (Phe) through pigment substitution of Bphe inside the proteins (see Scheme 1b for the molecular structure of Bphe and Phe). A long-lived P^+Bchl^- state and enhanced energy level of P^+Phe^- compared with that of P^+Bphe^- were confirmed by time-resolved spectroscopy [23–25]. However, the critical dependence of ET rate change on energy level shift of RC cofactors could hardly be obtained directly and readily.

In this work, wild-type RC (termed as WT-RC) and its plant Phe-exchanged mutant (termed as Phe-RC) isolated from purple bacterium *Rhodobacter sphaeroides* 601 were self-assembled on the functionalized Au electrodes. SWV and photoelectrochemical measurements were employed to systematically address the differences in the cofactor redox characters and photo-induced ET between the WT-RC films and the mutant ones. To our knowledge, it is the first time that the photo-induced ET difference arisen from RC mutagenesis was characterized directly by the photoelectric performance, owing to the great ability of SAMs in controlling the protein organization at the molecular level [16, 27] and facilitating the light-driven long-range ET [28, 29]. Combination of the advanced electrode modification strategies and the sensitive electrochemical methods provides a promising way for analyzing the primary events involved in the bacteria photosynthesis in detail.

Experimental section

Chemicals and material

2-Mercaptoacetic acid (MAA, Sigma, USA), polydimethyldiallylammonium chloride (PDDA, Aldrich, USA), and sodium dithionite (Dong-Huan United Chemical Plants, Beijing, China) were purchased without further purification. Other chemicals used in this study were analytical grade reagents. Deionized water with specific resistance ≥18 MΩ cm was adopted to prepare the solutions mentioned in this paper. Tris–HCl buffer (pH 8.0) employed in this study consisted of 0.050 M tris(hydroxymethyl)-aminomethane (Tris), 0.028 M HCl, and 0.050 M

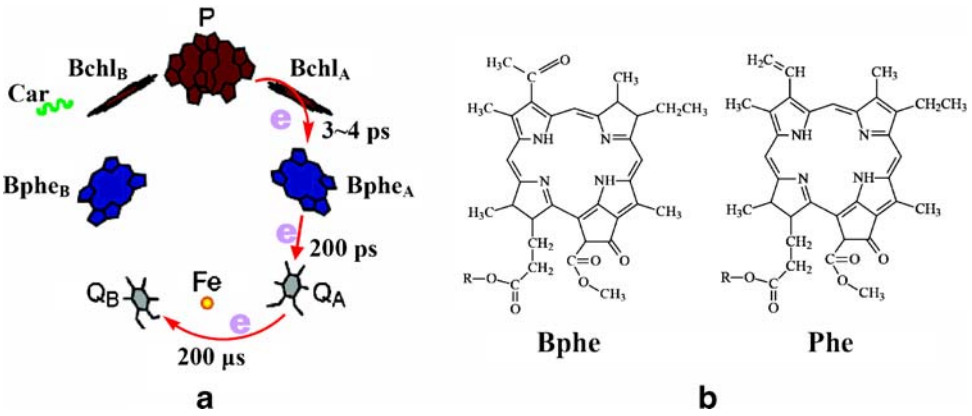

Scheme 1 **a** Photo-induced ET process of RC; **b** molecular structure of Bphe and Phe

KCl. Tris–LDAO (TL) buffer (pH 8.0) used in this study was composed of 10 mM Tris–HCl and 0.1% (*w*/*w*) lauryldimethylamine-*N*-oxide (LDAO).

Both WT-RC and Phe-RC were obtained from the Shanghai Institute of Plant Physiology and Ecology, Chinese Academy of Science. WT-RC was purified from the purple bacterium RS601 (one of *Rhodobacter sphaeroides* strain, containing carotenoid, with higher molecular weight than R26) according to the methods reported previously [30]. The purity index of the proteins was evaluated from the 280 and 802 nm absorption ratio (A_{280}/A_{800}), which should be less than 1.24. The concentration of RC was determined from the absorbance at 802 nm (molar extinction coefficient, ε=288 mM^{-1} cm^{-1}). Preparation of plant Phe and the process for pigment exchange were carried out as described previously [31]. In this work, Bphe at both the $Bphe_A$ and $Bphe_B$ sites was displaced by Phe with controlled molar proportion of Bphe and Phe as well as the incubation temperature. The $Phe_{A,B}$-exchanged mutant was obtained at a 20:1 Phe-to-RC molar ratio in 10% acetone, incubating at 43.5 °C for 60 min in the TL buffer.

Fabrication of RC–PDDA–MAA film on Au electrode

The details for constructing the RC–PDDA–MAA assembly were described as follows: Au electrode (surface area of about 0.038 cm^2, purchased from CHI Instrument, USA) was polished successively with 0.3 and 0.05 μm Al_2O_3 powder and washed gently with deionized water. Electrochemical characteristics of the bare Au electrode were estimated from the background current of CV ($\leq 2\times10^{-7}$ A in pH 8.0 Tris–HCl buffer at scan rate of 0.1 V/s) and SWV ($\leq 2\times10^{-7}$ A in pH 8.0 Tris–HCl buffer at 150 Hz). The freshly polished electrode was then ultrasonicated in deionized water and ethanol in turn for 3 min and finally rinsed thoroughly with ethanol. For realizing the modification, the above treated Au electrode was immersed in turn in 1 mg/ml MAA ethanol solution, 1 mg/l PDDA solution, and 0.5 mg/ml RC protein solution for 24, 6, and 3–4 h, respectively. After each step, the modified electrode was rinsed carefully and dried in nitrogen. A quartz crystal microbalance (QCM) was employed to investigate the surface concentration of RC in the SAMs if necessary. Before all measurements, the RC–PDDA–MAA assembly was rinsed and kept in pH 8.0 Tris–HCl buffer.

Apparatus and procedures

The ultraviolet (UV)-visible (Vis)-near infrared (NIR) absorption and fluorescence (FL) emission spectra were obtained using a SM-240 CCD spectrophotometer (CVI Spectral Instruments, Putnam, CT, USA.) and a SM-300 luminescence spectrometer (CVI Spectral Instruments, Putnam, CT, USA) at room temperature, respectively. The UV-Vis-NIR absorption and FL emission spectra of RC-free Tris–HCl buffer were subtracted automatically as reference or background. The QCM measurements were performed with a CHI-400 electrochemical crystal microbalance (CHI Instrument). The fundamental frequency of quartz resonators was 7.995 MHz. The geometrical area of the Au electrode used in the QCM measurements was 0.196 cm^2, and the roughness factor was about 1.45. The surface concentration of RC was determined by following the frequency change of the crystals and estimated using the Sauerbrey equation established for an AT-cut shear mode QCM [32]. In our system, per frequency change of 1 Hz represented the mass change of about 1.34 ng.

SWV measurements were carried out with a CHI-660A electrochemical workstation (CHI Instrument) at 295 K in the dark. All electrochemical experiments were performed within a three-electrode cell containing a RC-modified Au working electrode, a platinum flake auxiliary electrode, and a Ag/AgCl saturated KCl reference electrode. All the potentials quoted in this paper were vs standard hydrogen electrode (SHE). The electrolyte was purged with nitrogen for at least 20 min before the experiments and was kept in a nitrogen environment for exclusion of oxygen during all voltammetric scanning.

Nonlinear fitting of SWV data was applied to acquire the ET parameters (standard potential E°, rate constant k_s, and transfer coefficient α) [33]. This technology has been used to analyze the ET in thin myoglobin–phosphatidyl cholines (Mb–PC) successfully [34]. In this paper, the principle and program of SWV nonlinear fitting were the same as described previously [16].

The photocurrents were measured in a self-made quartz cell filled with 0.01 M sodium dithionite in pH 8.0 Tris–HCl buffer. A three-electrode system consisting of the RC-modified Au electrode as the working electrode, a saturated calomel electrode as the reference, and a platinum flake as the auxiliary one was adopted. A 20-W incandescent lamp coupled with a filter (λ>600 nm) was employed to illuminate the working electrode. The intensity (Iinc) of

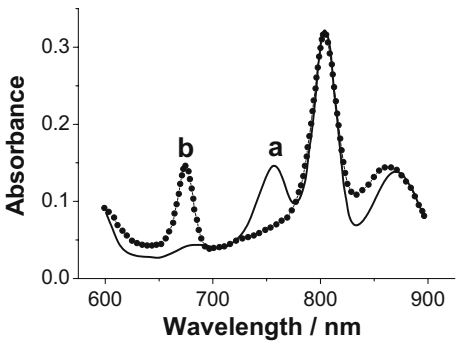

Fig. 1 Normalized NIR-Vis absorption spectra of WT-RC (*a*, *solid line*) and Phe-RC (*b*, *dotted line*) in pH 8.0 Tris–HCl buffer

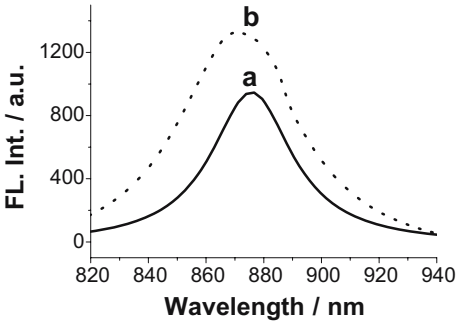

Fig. 2 Steady FL emission spectra of 2 μM WT-RC (*a*, *solid line*) and Phe-RC (*b*, *dotted line*) in pH 8.0 Tris–HCl buffer, excited at 800 nm

the output through the filter was measured to be 0.1 mW cm^{-2}. The photoelectric signals were recorded with the CHI-660A electrochemistry workstation mentioned above. Without extra illustration, the electrode bias was set at the open-circuit voltage during the photoelectric measurements.

Results and discussions

Steady absorption spectra

Figure 1 showed the differences of steady NIR absorption between WT-RC and Phe-RC in buffer resulted from pigment substitution. The normalized steady-state absorption spectra of the two kinds of RC were in good agreement with the previous results reported [23, 24]. For WT-RC, three major absorption peaks centered at 760, 802, and 870 nm corresponded to the Q_y transition for Bphe, Bchl, and P, respectively [35]. For Phe-RC, the peak of Bphe almost disappeared, while a new peak centered at 675 nm, corresponding to the Q_y absorption of Phe, was clearly identified. The results indicated that Bphe (at both the $Bphe_A$ and $Bphe_B$ sites) has been displaced successfully with Phe in the RC mutant, and a high exchange yield of more than 95% could be achieved. A blue-shift of 5 to 865 nm observed for Q_y transition of P in Phe-RC suggested the minor changes of band gap energy between P and its photoexcited state P*. The spectral characteristic of the monomeric Bchl molecules (802 nm) was not affected evidently by the pigment exchange.

Steady FL emission spectra

The FL emission spectra of 2 μmol/l WT-RC and Phe-RC excited at wavelength of 800 nm were displayed in Fig. 2 for comparison of the excitation relaxation of the two RC proteins. The FL intensity of Phe-RC was nearly 1.4 times larger than that of WT-RC. Similar results were observed when the excited light wavelength of 600 nm was employed. As the steady FL peak centered at ~875 nm (~871 nm for Phe-RC) can be definitely attributed to the emission of energy transferring from Bchl to P [36], the increased FL emission was mainly due to the slow-down formation of final charge-separated state in Phe-RC. These results also suggested the more population of P*, as reported previously by Schmidt et al. [24]. The somewhat higher free energy level of P^+Phe^- compared with that of P^+Bphe^- could be deduced.

QCM measurements for the WT-RC and Phe-RC SAMs

The surface concentration of RC in the RC–PDDA–MAA assembly was sensitively investigated by the QCM measurements. An average mass of the self-assembled WT-RC and Phe-RC was calculated to be 31.7 and 28.9 ng, respectively, as listed in Table 1. Compared with the results of polycation sandwiched RC SAMs reported in our previous work [16], the fabricated two RC assemblies in this work covered the gold electrode surface to a less extent. The protein mass calculated assumed a monolayer of RC adsorbed on the Au electrode [16]. No distinguished differences were found for the two kinds of RC SAMs on the surface coverage, which indicated that the protein matrix remained nearly unaltered after the pigment exchange.

Table 1 Electrochemical and photoelectrochemical parameters measured from nonlinear fitting of the SWVs with "5-$E°$" model and photoelectric tests, respectively[a,b,c]

Sample	M_{RC}/ng	E°/V			k_s/s^{-1}			α			I_{sc}/nA cm^{-2}	V_{oc}/mV
		I	II	III	I	II	III	I	II	III		
WT-RC SAMs	31.7	0.487	−0.08	−0.29	13.1	3.8	4.3	0.48	0.51	0.51	30	12
Phe-RC SAMs	28.9	0.511	−0.05	−0.32	14.0	3.1	3.4	0.53	0.52	0.54	45	17

[a] Mass of RC (M_{RC}) immobilized was obtained from the QCM measurements ($\Delta F=-7.46\times10^8$ Δm) with four times average; an error of ±5% was estimated.
[b] Standard potential $E°$, rate constant k_s, and transfer coefficient α were calculated from the SWVs (pulse heights of 50 mV and pulse frequency of 60 Hz) with an average of five times; an error of ±10% was estimated.
[c] Short-circuit photocurrent (Isc) and open circuit photovoltage (Voc) were measured with four times average (λ>600 nm).

SWV measurements for the WT-RC and Phe-RC SAMs

An attempt to follow the redox species involved in the ET reaction for the two RC SAMs was achieved by using the SWV, a potential method with superior sensitivity and resolution to CV. The reproducible and distinct electrochemical results shown in Fig. 3 demonstrated the change of redox reaction energetics and the partial block of ET process in Phe-RC. Three current peaks (marked as peak I, II, and III) were observed for both the two RC SAMs, while no redox peaks appeared for the bare Au or Au–MAA–PDDA electrodes. The well-characterized peaks and the following photocurrents responses exhibited the retaining of bioactivity of RC within the artificial films. According to the references in which the E_m of redox species in native RC has been widely reported to be 0.48~0.52 V for P/P^+ [37, 38], −0.05~−0.10 V for Q_A^-/Q_A [39, 40], and −0.3~−0.5 V for $Bphe^-$/Bphe [16]; peaks I, II, and III of the WT-RC SAMs in Fig. 3 corresponded affirmatively to the redox couples of P/P^+, Q_A^-/Q_A, and $Bphe^-$/Bphe, respectively. Similar results were obtained for the polycation sandwiched RC SAMs in our previous work [16]. Obvious changes of both peak potentials and currents were

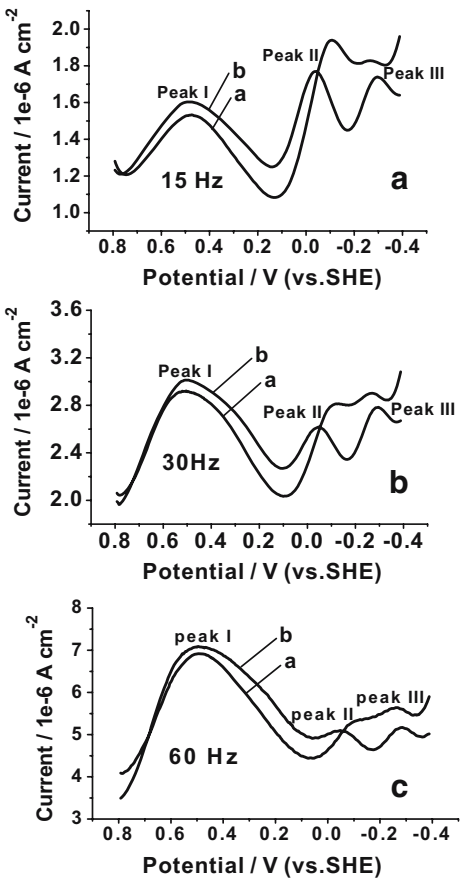

Fig. 3 Square wave voltammograms (*SWVs*) for the WT-RC SAMs (**a**) and Phe-RC SAMs (**b**) in pH 8.0 Tris–HCl buffer at 293 K with pulse amplitude of 25 mV and frequency of 15, 30, and 60 Hz applied

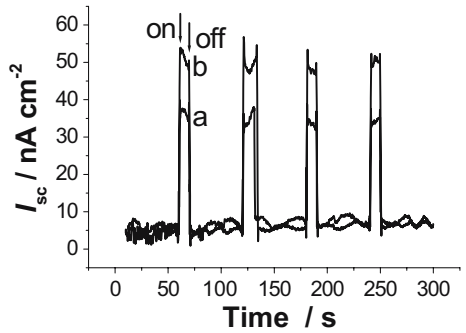

Fig. 4 Short-circuit photocurrent (*Isc*) responses induced by switching on (*arrow up*) and off (*arrow down*) the illumination (λ>600 nm, Iinc=0.1 mW cm^{-2}) of the RC–PDDA–MAA films on Au electrode. **a** WT-RC, (**b**) Phe-RC. The electrode potential was set at the open-circuit voltage

obtained for the Phe-RC SAMs, the details of which were described as follows. First, the enhanced current of peak I (P/P^+) for the mutant protein revealed a repopulation of the excited P* and a higher concentration of P^+ in Phe-RC, which was in good agreement with the results obtained by NIR absorption and FL emission spectra mentioned above. Second, the peak currents of peak II (Q_A^-/Q_A) and peak III (Phe^-/phe) for the Phe-RC SAMs, which were lower than those for the native one, was consistent with the results achieved by other groups. Franken et al. [25] reported that the yield of $P^+Q_A^-$ state was only 75% at room temperature in Phe-RC compared with nearly a unity in WT-RC. For Phe-RC SAMs, peak III was attributed to Phe^-/Phe mainly for the reason that the redox potential of this species in vitro was reported as a more negative value (130–160 mV) than that of Bphe in the same condition [41, 42]. The incorporation of Phe brought about the rise of free energy level of P^+Phe^-, which was higher than that of P^+Bchl^- in the RC mutant [23, 24], resulting in the increase of redox potential of peak III. In summary, it could be deduced that the ET from P to Q_A in the Phe-RC assembly was partly blocked as Phe-RC had higher concentration of P^+ (peak I) and lower yields of Q_A^- (peak II) compared with the native

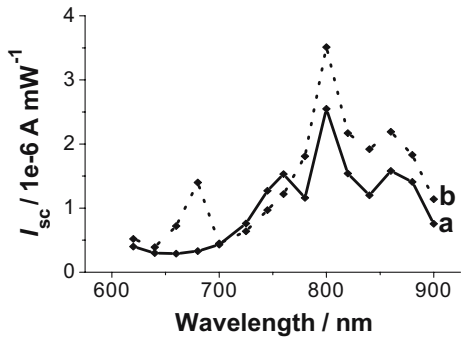

Fig. 5 Photocurrent action spectra of the WT-RC SAMs (*a*, *solid line*) and Phe-RC SAMs (*b*, *dotted line*) in the NIR region excited using a Ti–sapphire laser with tunable output of wavelength from 700~900 nm

one. The suppressant ET in Phe-RC was mainly attributed to the change of redox ET energetics.

Nonlinear fitting of the SWV data was performed to explain the electrochemical voltammetry differences between the WT-RC and Phe-RC SAMs quantitatively. Fitting of SWV data was done by nonlinear regression, a general program employing the Marquardt–Leenberg algorithm. Three parameters, including the $E°$, k_s, and α, were calculated from the regression analysis. The total fitting results for different RC–PDDA–MAA films are summarized in Table 1. The ET k_s of peak I for the WT-RC SAMs was calculated to be 13.1 s^{-1}, a little higher than the previous results reported for the iodoacetoamidyl–ubiquinone–RC films on carbon electrode [14]. The increased parallel k_s of about 14.0 s^{-1} was obtained for the Phe-RC one. Oppositely, the k_s of peak II (3.8 s^{-1}) and peak III (4.3 s^{-1}) estimated for the WT-RC SAMs was higher than the corresponding value for the Phe-RC one (3.1 and 3.4 s^{-1}, respectively). The different k_s presented in this paper further reflected the slow-down formation of final charge separation state in Phe-RC.

Photoelectric tests for the WT-RC and Phe-RC SAMs

Photoelectric performances of the WT-RC and Phe-RC SAMs were evaluated for directly differentiating the photo-induced ET behaviors of the two proteins, as shown in Fig. 4. No obvious photocurrent (<2 nA/cm^2) was observed for any RC-free Au or Au–MAA–PDDA electrodes photoexcited (λ>600 nm). However, reproducible anodic photocurrents were immediately observed for the two RC-modified electrodes when illuminated, which strongly indicated that the entrapped RC dominated the photocurrents. Short-circuit photocurrent (Isc) detected for the Phe-RC SAMs was near 45 nA/cm^2, about 1.5 times larger than that for WT-RC SAMs (~30 nA/cm^2). Meanwhile, enhanced open-circuit photovoltage (Voc) was also observed for the Phe-RC SAMs (see Table 1). As no significant differences on protein loading were found for the two RC SAMs, the dramatically different photoelectric performances implied the increased photo-induced electron injection for the Phe-RC SAMs compared with that for the native one. The enhanced photoelectric responses of the Phe-RC films were benefited from the more population and longer lifetime of P* or P^+Bchl^- in the mutant compared with that in the native. And the larger energy gap existed between P* or P^+BChl^- and P/P^+ than that between $P^+Q_A^-$ and P/P^+ also contributed to the photoelectric performance difference. Photocurrent of the WT-RC and Phe-RC SAMs as a function of the NIR illumination light wavelength is illustrated in Fig. 5. The photocurrent action spectra of the two electrodes almost overlay the absorption spectra of the two proteins, which confirmed again that the photocurrents measured in the NIR region were indeed generated by the entrapped RC, and the NIR light-harvesting capability of both WT-RC and Phe-RC in the SAMs was well preserved. Enhanced photoelectric performances observed in the Q_y absorption bands of P and Bchl for the Phe-RC SAMs further mapped the connection between the energy level change of the redox cofactors and the photo-induced ET process.

Conclusions

Pigment substitution led to the significant alterations on the cofactor redox characters and photo-induced ET process of the bacteria photosynthetic proteins, which were probed by the NIR-Vis absorption, FL emission, SWV, and photoelectrochemical experiments. Different ET process in the two SAMs contributed to the differences in electrochemical and photoelectrochemical behavior. The electrochemical results exhibited that ET initiated by the oxidation of P was obviously slowed down and P^+ formed had more population as well as more positive E_m in the Phe-RC films compared with those in the WT ones. The dramatically enhanced photoelectric performances of the mutant RC further suggested convincingly the formation of relatively long-lived P* and P^+Bchl^- in Phe-RC. The unique protein films introduced in this study provided an efficient approach to sensitively probe the redox cofactors and ET differences resulting from only minor changes in pigment arrangement in the pigment–protein complex. The favored ET process observed for the membrane proteins RC was potentially valuable for a deep understanding of the multi-step biological ET and development of versatile bioelectronic devices.

Acknowledgment This work was supported by NSFC (20335040, 20525519, 90606014, and 20605005).

References

1. Marcus RA (1993) Angew Chem Int Ed Engl 32:1119
2. Moser CC, Keske JM, Warncke K, Farid RS, Dutton PL (1992) Nature 355:796
3. Feher G, Allen JP, Okamura MY, Rees DC (1989) Nature 339:111
4. Kirmaier C, Gaul D, Debey R, Holten D, Schenck CC (1991) Science 251:922
5. Blankenship RE, Madigan MT, Bauer CE (1995) Kluwer, Dordrecht, The Netherlands
6. Allen JP, Williams JC (1998) FEBS Lett 438:5
7. Van Brederode ME, Van Grondelle R (1999) FEBS Lett 455:1
8. Hoff AJ, Deisenhofer (1997) J Phys Rep 287:2
9. Stowell MHB, MxPhilips TM, Rees DC, Soltis SM, Abresch E, Feher G (1997) Science 276:812
10. Kriegl JM, Nienhaus GU (2004) Proc Natl Acad Sci U S A 101:123

11. Cosma P, Longobardi F, Agostiano A (2004) J Electroanal Chem 564:35
12. Agostiano A, Caselli M, Cosma P, Monica MD (2000) Electrochim Acta 45:1821
13. Munge B, Pendon Z, Frank HA, Rusling JF (2001) Bioelectrochemistry 54:145
14. Katz E (1994) J Electroanal Chem 365:157
15. Kong JL, Lu ZQ, Lvov YM, Desamero RZB, Frank HA, Rusling JF (1998) J Am Chem Soc 120:7371
16. Kong JL, Sun WL, Wu XL, Deng JQ, Lu ZQ, Lvov YM, Desamero RZB, Frank HA, Rusling JF (1999) Bioelectrochem Bioenerg 48:101
17. Zhao JQ, Zhou YL, Liu BH, Xu CH, Kong JL (2002) Biosens Bioelectron 17:711
18. Lu YD, Yuan MJ, Liu Y, Tu B, Xu CH, Liu BH, Zhao DY, Kong JL (2005) Langmuir 21:4071
19. Lu YD, Xu JJ, Liu Y, Liu BH, Xu CH, Zhao DY, Kong JL (2006) Chem Commun 7:785
20. Beekmen LMP, Van Stokkum IHM, Monshouwer R, Rijnders AJ, McGlynn P, Visschers RW, Jones MR, Van Grondelle R (1996) J Phys Chem 100:7256
21. Haffa ALM, Lin S, Katilius E, Williams JC, Taguchi AKW, Allen JP, Woodbury NW (2002) J Phys Chem B 106:7376
22. Schenkl S, Sporlein S, Muh F, Witt H, Lubitz W, Zinth W, Wachtveitl J (2002) Biochim Biophys Acta 1554:36
23. Kennis JTM, Shkuropatov AY, Van Stokkum IHM, Gast P, Hoff AJ, Shuvalov VA, Aartsma TJ (1997) Biochemistry 36:16231
24. Schmidt S, Arlt T, Hamm P, Huber H, Nagele T, Wachtveitl J, Zinth W, Meyer M, Scheer H (1995) Spectrochim Acta Part A 51:1565
25. Franken EM, Shkuropatov AY, Francke C, Neerken S, Gast P, Shuvalov VA, Hoff AJ, Aartsma TJ (1997) Biochim Biophys Acta 1321:1
26. Shkuropatov AY, Neerken S, Permentier HP, Wijn RD, Schmidt KA, Shuvalov VA, Aartsma TJ, Gust P, Hoff AJ (2003) Biochim Biophys Acta 1557:1
27. Tasayco ML, Carey J (1992) Science 255:594
28. Imahori H, Fukuzumi S (2001) Adv Mater 13:1197
29. Yanagisawa K, Morita T, Kimura S (2004) J Am Chem Soc 126:12780
30. Zeng XH, Yu H, Wu YQ, Wu MG, Wei JM, Song HY, Xu CH (1997) Acta Biochim Biophys Sinica 29:46
31. Zeng XH, Wu YQ, Shen YG, Xu CH (2000) Sci China Ser C 43:21
32. Buttry DA, Ward MD (1992) Chem Rev 92:1355
33. O'Dea JJ, Osteryoung J (1993) Anal Chem 65:3090
34. Zhang Z, Rusling JF (1997) Biophys Chem 63:133–146
35. Arnett DC, Moser CC, Dutton PL, Scherer NF (1999) J Phys Chem B 103:2014
36. Wright CA, Clayton RK (1973) Biochim Biophys Acta 333:246
37. Moss DA, Leonhard M, Bauscher M, Mantele W (1991) FEBS Lett 283:33
38. Ivancich A, Artz K, Williams JC, Allen JP, Mattioli TA (1998) Biochemistry 37:11812
39. Alegria G, Dutton PL (1991) Biochim Biophys Acta 1057:239–257
40. Crofts AR, Wraight CA (1983) Biochim Biophys Acta 726:149
41. Schmidt S, Arlt T, Hamm P, Huber H, Nagele T, Wachtveitl J, Meyer M, Scheer H, Zinth W (1994) Chem Phys Lett 223:116
42. Huber H, Meyer M, Nagele T, Hartl I, Scheer H, Zinth W, Wachtveitl (1995) J Chem Phys 197:297